Published Online: 2 May, 2023 | Supp Info: http://doi.org/10.26508/lsa.202201730


Research Article

TRANSPARENT PROCESS SOURCE DATA OPEN ACCESS

Life Science Alliance



# Deletion of SERF2 in mice delays embryonic development and alters amyloid deposit structure in the brain

Esther Stroo[1]*, Leen Janssen[1]*, Olga Sin[1,2], Wytse Hogewerf[1], Mirjam Koster[3], Liesbeth Harkema[3], Sameh A Youssef[3,4], Natalie Beschorner[5], Anouk HG Wolters[6], Bjorn Bakker[1], Lore Becker[7], Lilian Garrett[7,8], Susan Marschall[7], Sabine M Hoelter[7,8,9], Wolfgang Wurst[8,10,11,12], Helmut Fuchs[7], Valerie Gailus-Durner[7], Martin Hrabe de Angelis[7,13,14], Amantha Thathiah[15,16], Floris Foijer[1], Bart van de Sluis[3], Jan van Deursen[17], Matthias Jucker[5], Alain de Bruin[3,4], Ellen AA Nollen[1]

In age-related neurodegenerative diseases, like Alzheimer's and Parkinson's, disease-specific proteins become aggregation-prone and form amyloid-like deposits. Depletion of SERF proteins ameliorates this toxic process in worm and human cell models for diseases. Whether SERF modifies amyloid pathology in mammalian brain, however, has remained unknown. Here, we generated conditional *Serf2* knockout mice and found that full-body deletion of *Serf2* delayed embryonic development, causing premature birth and perinatal lethality. Brain-specific *Serf2* knockout mice, on the other hand, were viable, and showed no major behavioral or cognitive abnormalities. In a mouse model for amyloid-β aggregation, brain depletion of *Serf2* altered the binding of structure-specific amyloid dyes, previously used to distinguish amyloid polymorphisms in the human brain. These results suggest that *Serf2* depletion changed the structure of amyloid deposits, which was further supported by scanning transmission electron microscopy, but further study will be required to confirm this observation. Altogether, our data reveal the pleiotropic functions of SERF2 in embryonic development and in the brain and support the existence of modifying factors of amyloid deposition in mammalian brain, which offer possibilities for polymorphism-based interventions.

DOI 10.26508/lsa.202201730 | Received 20 September 2022 | Revised 18 April 2023 | Accepted 18 April 2023 | Published online 2 May 2023

## Introduction

Protein aggregation is a pathological hallmark shared by several age-related neurodegenerative diseases, such as Alzheimer's (AD), Parkinson's, and Huntington's diseases. The amyloid-like aggregates that accumulate in each of these diseases are composed of disease-specific proteins, that is, amyloid-beta (A ) and tau in AD (Glenner & Wong, 1984; Masters et al, 1985; Grundke-Iqbal et al, 1986a, 1986b) or alpha-synuclein ( -Syn) in Parkinson's disease (Spillantini et al, 1997). Although the exact molecular mechanisms underlying the disease pathology remain to be elucidated, genetic evidence indicates that these aggregation-prone proteins play a key role in the disease processes. Mutations altering the production, processing, and folding of these proteins are sufficient to cause these diseases (Citron et al, 1992; Suzuki et al, 1994; Haass et al, 1995; Borchelt et al, 1996; Duff et al, 1996; Conway et al, 1998, 2000; Cooper et al, 1998; Murayama et al, 1999; Narhi et al, 1999; Miravalle et al, 2000; Murrell et al, 2000; Nilsberth et al, 2001; Choi et al, 2004; Tomiyama et al, 2008; Ni et al, 2011; Ghosh et al, 2013, 2014). Mechanisms underlying age-related protein aggregation include protein homeostatic mechanism that appear to decline with age, which are well studied with the underlying idea that boosting these mechanisms could prevent or delay disease (Labbadia & Morimoto, 2015; Boland et al, 2018; Hipp et al, 2019; Alberti & Hyman, 2021). In contrast, little is known about cellular

[1]European Research Institute for the Biology of Ageing, University of Groningen, University Medical Centre Groningen, Groningen, The Netherlands [2]Graduate Program in Areas of Basic and Applied Biology, Instituto de Ciências Biomédicas Abel Salazar, Universidade do Porto, Porto, Portugal [3]Department of Biomolecular Health Sciences, Faculty of Veterinary Medicine, Utrecht University, Utrecht, The Netherlands [4]Department of Pediatrics, Molecular Genetics Section, University of Groningen, University Medical Centre Groningen, Groningen, The Netherlands [5]Department of Cellular Neurology, Hertie-Institute for Clinical Brain Research, University of Tübingen, Tübingen, Germany [6]Department of Biomedical Sciences of Cells and Systems, University Medical Centre Groningen, Groningen, The Netherlands [7]Institute of Experimental Genetics, German Mouse Clinic, Helmholtz Zentrum München, German Research Center for Environmental Health (GmbH), Neuherberg, Germany [8]Institute of Developmental Genetics, Helmholtz Zentrum München, German Research Center for Environmental Health, Neuherberg, Germany [9]Technische Universität München, Freising-Weihenstephan, Germany [10]Chair of Developmental Genetics, TUM School of Life Sciences, Technische Universität München, Freising-Weihenstephan, Germany [11]Deutsches Institut für Neurodegenerative Erkrankungen (DZNE) Site Munich, Munich, Germany [12]Munich Cluster for Systems Neurology (SyNergy), Adolf-Butenandt-Institut, Ludwig-Maximilians-Universität München, Munich, Germany [13]Chair of Experimental Genetics, TUM School of Life Sciences, Technische Universität München, Freising, Germany [14]German Center for Diabetes Research (DZD), Neuherberg, Germany [15]VIB Center for the Biology of Disease, KU Leuven Center for Human Genetics, University of Leuven, Leuven, Belgium [16]Department of Neurobiology, University of Pittsburgh Brain Institute, University of Pittsburgh School of Medicine, Pittsburgh, PA, USA [17]Mayo Clinic, Rochester, MN, USA

Correspondence: l.l.s.janssen@umcg.nl; e.a.a.nollen@umcg.nl
*Esther Stroo and Leen Janssen contributed equally to this work

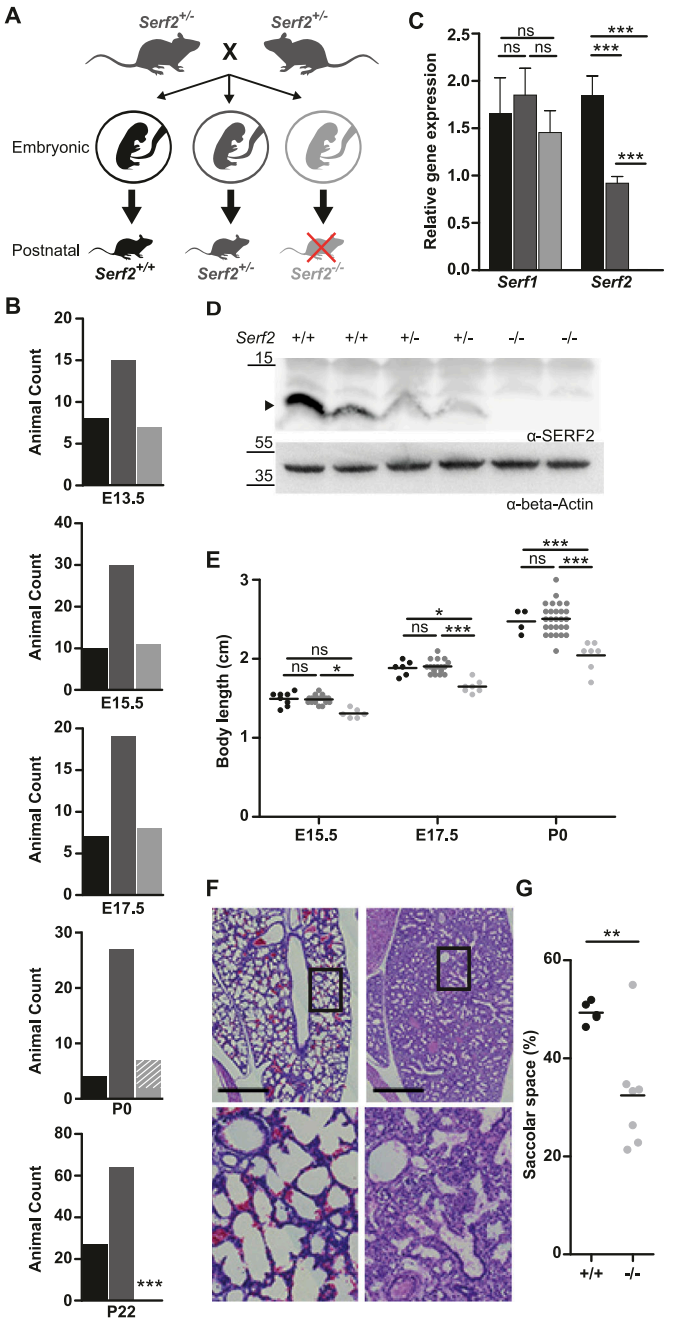


Figure 1. Full-body ***Serf2***$^{-/-}$ mice display a developmental delay and perinatal lethality.
(A) Schematic overview of the crossing scheme with full-body Serf2$^{+/-}$ mice and the resulting genotypic composition of the offspring at the embryonic and postnatal stages. (B) Absolute animal counts for the three genotypes in the offspring at various days of embryonic development (E13.5, E15.5, and E17.5), at birth (P0) and at time of weaning (P22). (C) Real time RT-PCR analyses of Serf1 and Serf2 RNA levels in E13.5 heads normalized to housekeeping gene-actin (n = 4/group, mean ± SD, one-way ANOVA for each gene, Bonferroni corrected post-hoc comparison between genotypes $^{ns}p_{bon} > 0.05$, $^{***}P < 0.001$) (D) Western blot of SERF2 and actin in Serf2$^{+/+}$, Serf2$^{+/-}$, Serf2$^{-/-}$ embryos at E13.5 (black arrow indicates the SERF2 band) (E) Length measurements of Serf2$^{+/+}$, Serf2$^{+/-}$, Serf2$^{-/-}$ embryos at E15.5, E17.5, and P0 (black line = mean, two-way ANOVA with factor age and genotype, Bonferroni corrected post-hoc comparison for Serf2$^{+/-}$ and Serf2$^{-/-}$ compared with Serf2$^{-/-}$ $^{ns}p_{bon} > 0.05$, $^{*}P < 0.05$; $^{***}P < 0.001$). (F) Hematoxylin and eosin stained lung tissue from Serf2$^{+/+}$ and Serf2$^{-/-}$ pups at P0 (left: Serf2$^{+/+}$, right: Serf2$^{-/-}$, scale bar = 500 m, rectangle = 5× magnification in bottom picture). (G) Quantification of the saccolar space in lung tissue from Serf2$^{+/+}$ and Serf2$^{-/-}$ pups at P0 (black line = mean, t test $^{**}P < 0.01$). For all mouse data panels: Serf2$^{+/+}$ = black, Serf2$^{+/-}$ = dark grey, Serf2$^{-/-}$ = light grey.
Source data are available for this figure.

mechanisms that drive toxicity and aggregation of aggregation-prone proteins. Inhibiting such driving mechanisms could provide an alternative and complementary approach to treat protein conformational diseases.

Through a genetic screen in Caenorhabditis elegans (C. elegans), a highly charged cellular protein has been identified that has the capacity to enhance protein toxicity and aggregation of multiple disease-related, aggregation-prone proteins (van Ham et al, 2010). This peptide was dubbed modifier of aggregation-4 (MOAG-4) and was found to be an ortholog of two human proteins: SERF1A and SERF2. Interestingly, SERF proteins accelerate the aggregation of multiple amyloidogenic proteins in vitro, but not non-amyloidogenic proteins (Falsone et al, 2012; Yoshimura et al, 2017; Pras et al, 2021). This aggregation-promoting effect has been accredited to the interaction of a highly positively charged N-terminal segment with segments of the aggregation-prone proteins that are enriched in negatively charged and hydrophobic aromatic amino acids leading to the disruption of its inter and intramolecular electrostatic interactions (Yoshimura et al, 2017; Merle et al, 2019; Meyer et al, 2020; Pras et al, 2021). Neutralizing the charge of MOAG-4 and SERF2 in this N-terminal segment is sufficient to suppress their effect on aggregation and to reduce toxicity in C. elegans models for polyglutamine and A pathology (Pras et al, 2021). In this study, we use the established APPPS1-21 mouse model for A-pathology to investigate whether the removal of SERF2 also modifies the aggregation of amyloidogenic proteins in the more biologically complex environment of the mammalian brain.

## Results

### Full-body Serf2 KO results in developmental delay and perinatal lethality in mice

To establish the role of SERF2 in vivo, we first ensured SERF2 expression in all major organs, including the brain, and proceeded to generate full-body Serf2 knockout (KO) mice (Fig S1A–C). During an initial cross, using the four homozygous Serf2 KO animal (Serf2$^{-/-}$) and eight heterozygous Serf2 KO animals (Serf2$^{+/-}$) we obtained, only one Serf2$^{-/-}$ survived the day of birth compared with 27 Serf2$^{+/-}$ and 96 Serf2 wild-type (Serf2$^{+/+}$) mice (Table S1). After backcrossing into C57BL/6J background, interbreeding of Serf2$^{+/-}$ animals did not result in any viable Serf2$^{-/-}$ mice at the time of weaning (Fig 1A and B). To determine whether Serf2$^{-/-}$ mice died during fetal development, we examined the offspring at multiple developmental stages: embryonic days 13.5, 15.5, and 17.5. In all of the examined embryonic stages, we observed the expected Mendelian ratio of genotypes, around 25% Serf2$^{+/+}$ and Serf2$^{-/-}$ embryos and around 50% Serf2$^{+/-}$ (Chi Square: E13.5 $P = 0.9672$; E15.5 $P = 0.4432$; E17.5 $P = 0.7674$), indicating unaltered viability during embryonic

development (Fig 1B). At birth (P0), however, all Serf2$^{-/-}$ displayed respiratory distress and the majority (5/7) died within 30 min of being born. At the time of weaning, the Mendelian ratio was maintained between the Serf2$^{+/+}$ and Serf2$^{+/-}$ animals, but no Serf2$^{-/-}$ mice survived until this stage (Chi Square: P22 $P < 0.0001$). At E13.5 Serf2 mRNA levels showed a 50% reduction for Serf2$^{+/-}$ and complete KO for Serf2$^{-/-}$ compared with Serf2$^{+/+}$ (One-way ANOVA: between all three genotypes $p_{Bon} < 0.0001$) (Fig 1C). No compensatory change in Serf1 mRNA levels was observed, suggesting that they function independently from each other (One-way ANOVA: $P = 0.2403$) (Fig 1C). A similar ratio in SERF2 expression was also observed on the protein level (Fig 1D).

Further analysis to uncover the cause of this perinatal lethality revealed an increasing difference in the embryo size of Serf2$^{-/-}$ compared with Serf2$^{+/+}$ and Serf2$^{+/-}$ from E15.5 until birth (Two-way ANOVA body length: E15.5 Serf2$^{-/-}$ versus Serf2$^{+/-}$ $p_{Bon} = 0.0419$, Serf2$^{-/-}$ versus Serf2$^{+/+}$ $p_{Bon} = 0.0874$; E17.5 Serf2$^{-/-}$ versus Serf2$^{+/-}$ $p_{Bon} = 0.0003$, Serf2$^{-/-}$ versus Serf2$^{+/+}$ $p_{Bon} = 0.0157$; P0 Serf2$^{-/-}$ versus Serf2$^{+/-}$ and Serf2$^{+/+}$ $p_{Bon} < 0.0001$) (Fig 1E) (Two-way ANOVA body mass: E17.5 Serf2$^{-/-}$ versus Serf2$^{+/-}$ $p_{Bon} = 0.0124$, Serf2$^{-/-}$ versus Serf2$^{+/+}$ $p_{Bon} = 0.2381$; P0 Serf2$^{-/-}$ versus Serf2$^{+/-}$ and Serf2$^{+/+}$ $p_{Bon} < 0.0001$) (Fig S1D and E). No differences in size could be observed between homozygous wild-type Serf2$^{+/+}$, and heterozygous Serf2$^{+/-}$ embryos at any embryonic stage, including P0

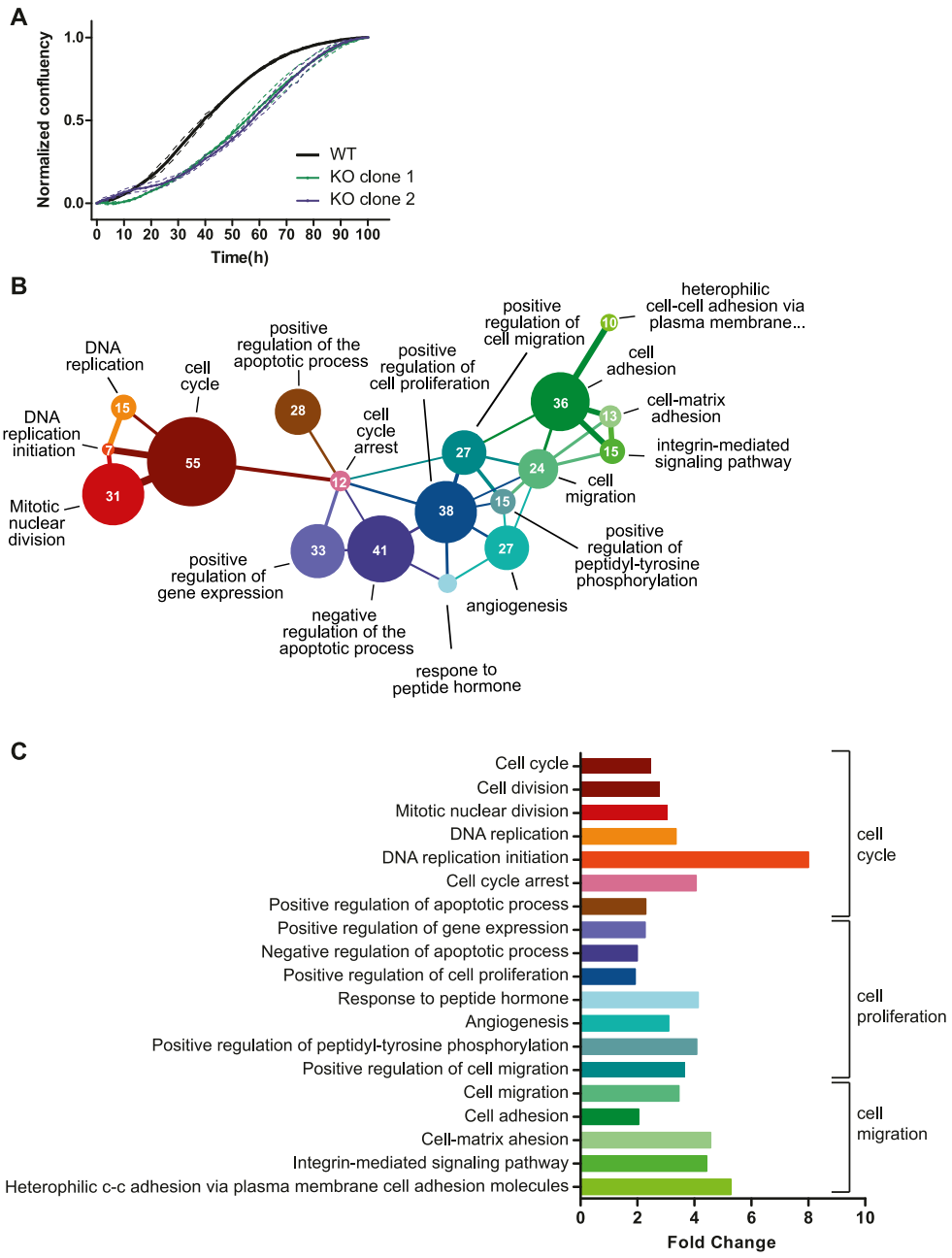


Figure 2. Cell culture data of ***Serf2*** KO and control HEK cells and RNA sequencing analysis of MEFs isolated from full-body ***Serf2***$^{-/-}$ and control mice.
(A) Growth curve of two CRISPR-induced Serf2$^{-/-}$ clones of HEK293T versus wild-type HEK293T. (Three replicates measured, full line = replicate average, dashed lines = SD on average). (B) Network showing the interconnectivity of enriched GO terms in RNA sequencing data from Serf2$^{-/-}$ and control MEFs. Circle size indicates the amount of differentially expressed genes found in each GO category. Edges were drawn when the minor category shared more than 25% of its found genes with the major category. Edge color indicates the major category in the relationship. Edge thickness indicates the percentage of found genes shared by the minor category. (C) Bar chart indicating the fold change for each GO term as determined by DAVID (B) Brackets indicate the three main GO term clusters defined based on the network in (B).
Source data are available for this figure.

(Two-way ANOVA for both body length and weight: at all ages $p_{bon} > 0.9999$). We excluded placental abnormalities, causing an impaired transfer of nutrients and oxygen to the embryo as a cause for the growth delays (Ward et al, 2012). Examination of placenta at all three embryonic stages for microscopic lesions in the placental labyrinth or other changes revealed no genotype-related pathology of the placenta. The results suggest that the absence of SERF2 in the embryo itself was responsible for the observed growth phenotype. Histological examination of various tissues revealed a developmental delay of ~1–2 d in the organs of E17.5 $Serf2^{-/-}$ embryos compared with the previous time points and standard embryonic development (Kaufman, 1992; Kaufman & Bard, 1999). This was most prominent in the lungs, through reduced expansion of alveoli and augmented tissue density (Fig 1F), and in the kidneys, by the increased amount of mesenchyme between the tubules and glomeruli (Fig S1F). At the time of birth, the lungs of $Serf2^{-/-}$ pups displayed a significantly reduced saccular space (*t* test: P = 0.0088) (Fig 1G), reflecting insufficient lung expansion and maturation. This phenomenon, called partial fetal atelectasis, seems to explain the observed respiratory distress and is a likely cause of the perinatal lethality in $Serf2^{-/-}$ pups.

## SERF2 affects growth in a cell-autonomous manner

Given the ubiquitous expression of SERF2 and its overall effect on growth, we examined whether the effect could be cell intrinsic. We generated CRISPR-induced $Serf2^{-/-}$ HEK293T clonal cell lines and found that they also display slower proliferation (Fig 2A). Moreover, RNA sequencing analysis of MEF isolated from E13.5 embryos showed a clear enrichment of GO-terms clustered around three closely related biological functions: cell cycle, cell proliferation, and cell adhesion (Fig 2B and C). Interestingly, in the cell cycle cluster, we observe an overall up-regulation of factors driving cell division and down-regulation of growth arrest factors in $Serf2^{-/-}$ MEFs (Table S2). The up-regulation of cell cycle regulators may seem counterintuitive in cells that divide slower. However, the up-regulation of cell cycle factor does not automatically mean that cells divide faster. It could be that they need longer time to passage through S or G2 because they experience replication stress and need to repair DNA in the G2 phase. This leads to up-regulation of cell cycle factors as well because they need longer time to passage through these phases. This observation also seems in line with a developmental delay phenotype in $Serf2^{-/-}$ mice, because it is known that cell proliferation is favored over differentiation in earlier stages of embryonic development compared with later stages (Ciemerych & Sicinski, 2005). Overall, the cell culture results point towards a cell-autonomous effect of SERF2 and suggest that deletion of *Serf2* delays cell growth, which is consistent with a previous report (Tsuboyama et al, 2020). Although our previous study also demonstrated a cell-autonomous function in regulating protein aggregation for MOAG-4, we did not find visible effects of MOAG-4 deletion on the viability or life span of *C. elegans* (van Ham et al, 2010). Altogether, our results suggest that the perinatal lethality caused by *Serf2* KO is because of the delayed maturation of certain organs.

## Conditional Serf2 KO mice display a reduction in size, but no other structural abnormalities in the brain

Going back to our initial aim to establish the effect of SERF2 depletion on amyloid aggregation in mouse brain, we needed to circumvent the perinatal lethality of full-body *Serf2* KO mice. We therefore generated a brain-specific *Serf2* KO mouse model ($Serf2^{br-/-}$) by combining our $Serf2^{flox/flox}$ mice with the Sox1-Cre model (Takashima et al, 2007) (Fig 3A). Brain-specific KO of *Serf2* were indeed viable (Chi Square: P = 0.37) (Table S3). Analysis of *Serf2* expression on the mRNA in various organs and on the protein level confirmed brain-specific ablation of *Serf2* by Sox1-mediated Cre

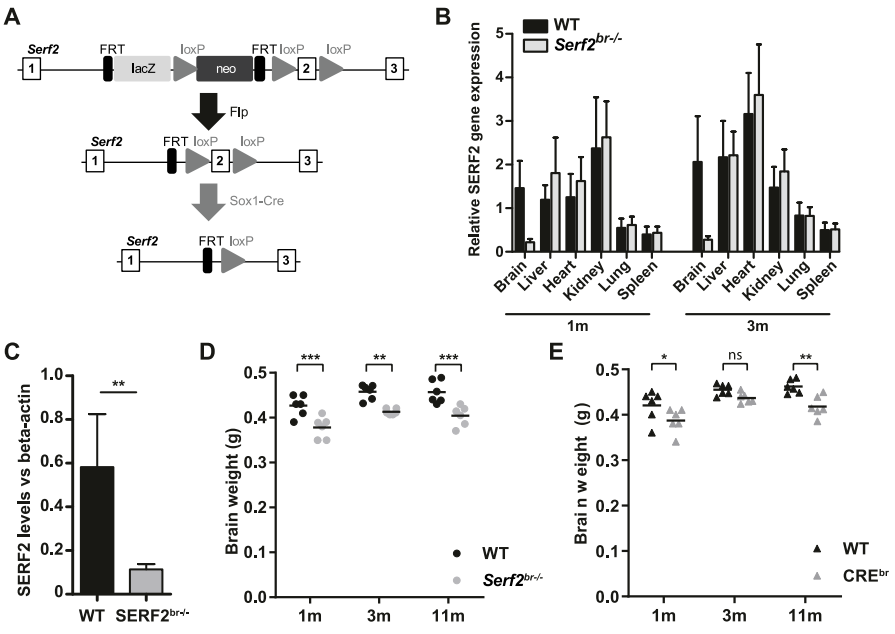


Figure 3. Brain-specific conditional KO results in reduced brain weight, partially attributed to Cre-expression.
(A) Modified targeting strategy used to delete the exon 2 of *Serf2* specifically in the central nervous system.
(B) Real time RT-PCR analyses of *Serf2* RNA expression in different organs $Serf2^{+/+}$ and $Serf2^{br-/-}$ female mice at 1 and 3 mo of age. *Serf2* expression was normalized to housekeeping gene β-actin (all groups n = 6, mean ± SEM). (C) Quantification of *Serf2* and β-actin Western blot analysis in brain lysates of WT and $Serf2^{br-/-}$ female mice at 1 mo (both groups n = 6, mean ± SEM, *t* test $^{**}P < 0.01$). (D) Evolution of brain weight in WT and $Serf2^{br-/-}$ female mice between 1 and 11 mo of age. (E) Brain weight of unfloxed WT and $CRE^{br}$ mice between 1 and 11 mo of age. For panel (D, E): black line = mean, two-way ANOVA with factors such as age and genotype, Bonferroni corrected post-hoc for genotype comparison at each age $^{ns}p_{bon} > 0.05$, $^{*}p_{bon} < 0.05$, $^{**}p_{bon} < 0.01$, $^{***}p_{bon} < 0.001$.
Source data are available for this figure.

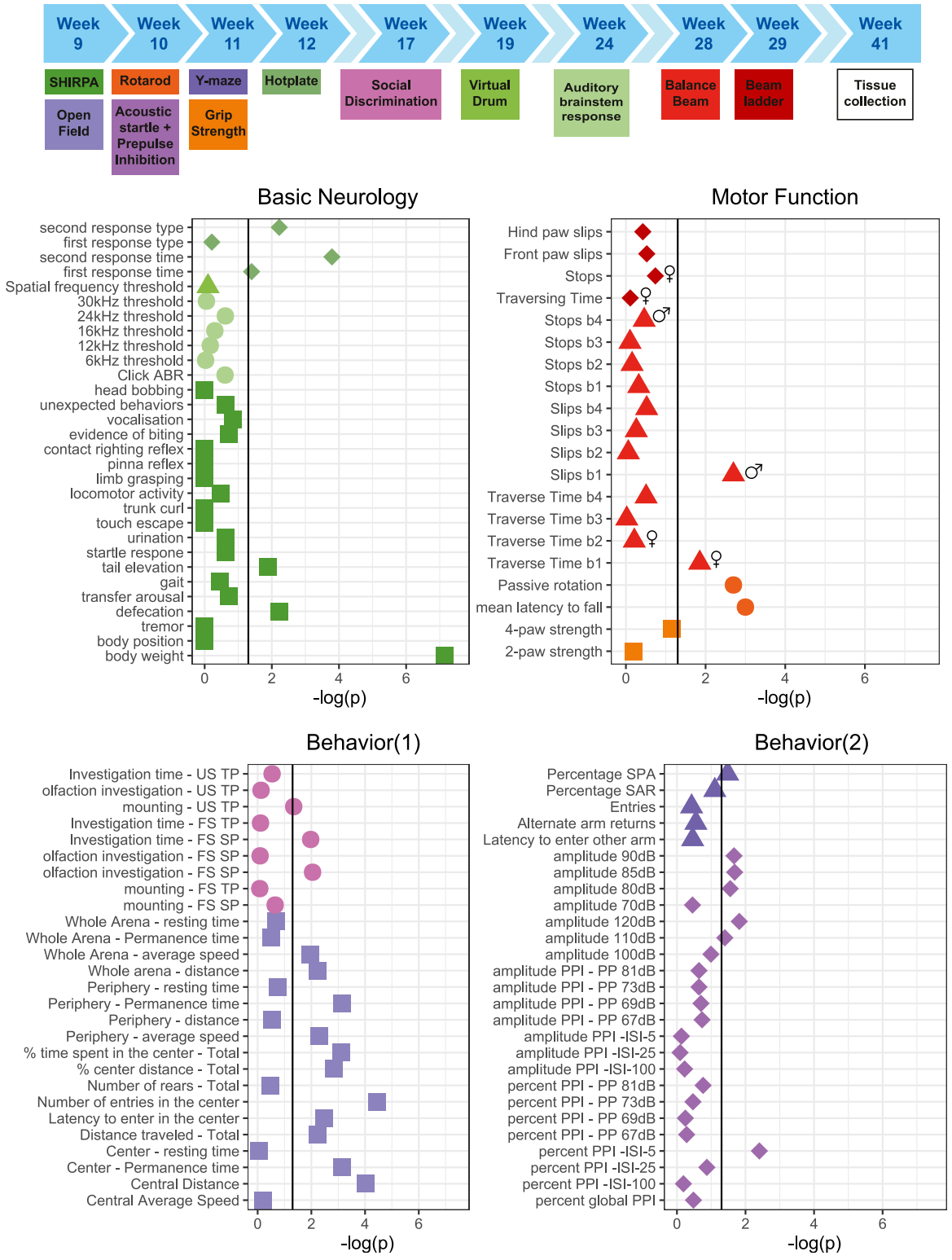


Figure 4. Extensive phenotyping of conditional ***Serf2*** KO mice reveals reduced body weight and some subtle behavioral changes, but no clear neurological or motor function defects.
The top panel provides a schematic overview of the complete phenotyping pipeline used and the ages of testing. The mice were used from a separate breeding line, dedicated to behavioral testing. An overview of the test results is grouped in the four bottom panels according to the three general modalities investigated: basic neurological functioning, overall motor function, and behavior. Graphs show the −log (P-value) for the comparison between WT and $Serf2^{tm1b/+}$ mice for all parameters tested (vertical black line = significance level of 0.05, sex symbols indicate that sex-specific analysis of the parameter only revealed a significant difference for sex). Source data are available for this figure.

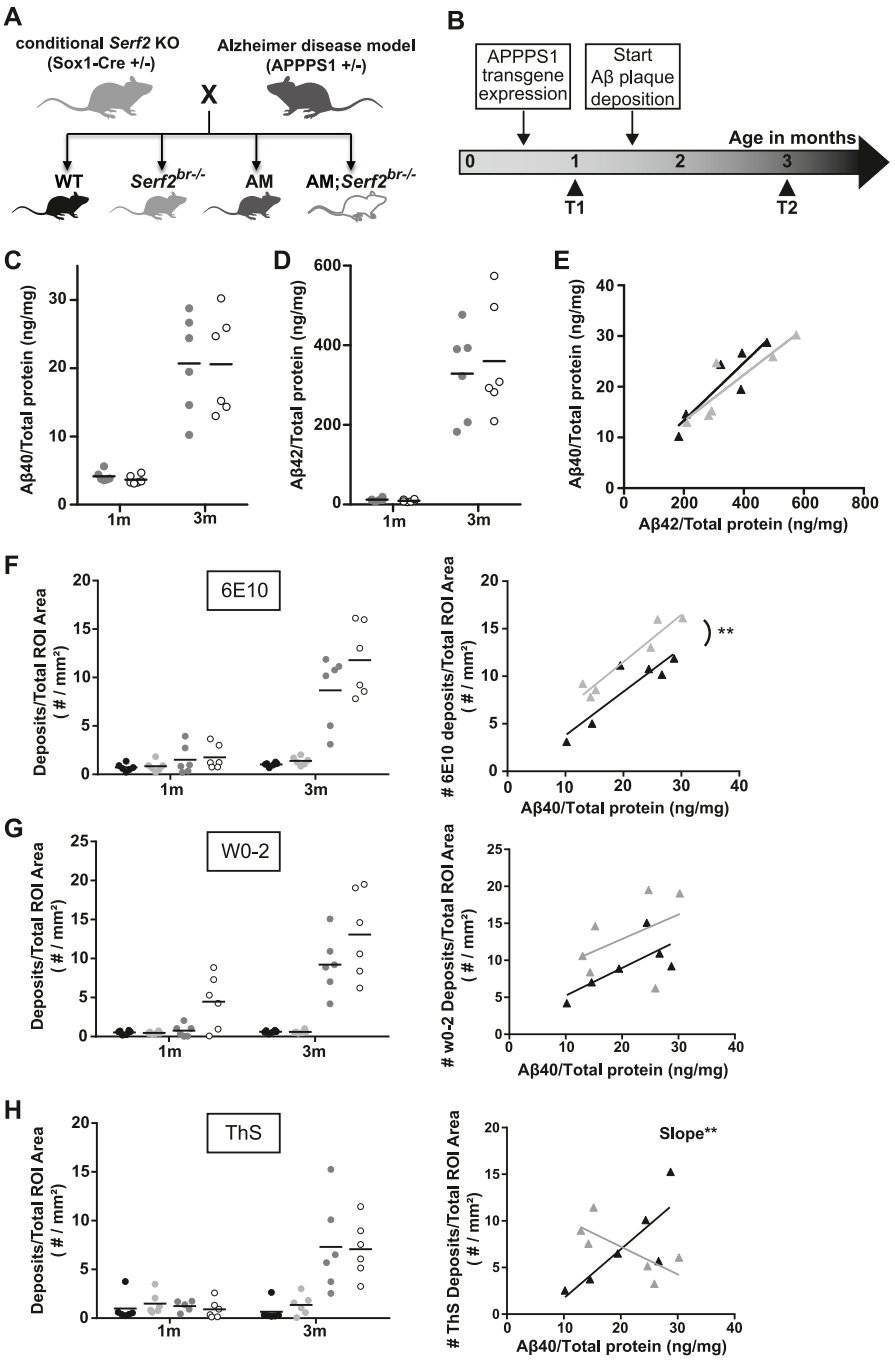


Figure 5. Crossing a conditional *Serf2* KO with an AM background does not affect A $\beta$ levels, but modifies A$\beta$ plaque formation.
(A) Schematic overview of the cross between brain-specific Serf2 KO mice and the amyloid model resulting in four experimental groups: WT, Serf2$^{br-/-}$, AM, and AM;Serf2$^{br-/-}$. (B) Timeline for the A pathology in the amyloid model and the selected time points for this study. (C, D) A$_{40}$ and (D) A$_{42}$ levels in brain lysate from AM and AM;Serf2$^{br-/-}$ mice at 1 and 3 mo of age as determined by ELISA normalized to total protein content. (black line = mean, t test between genotypes at both ages not significant). (E) Correlation plot depicting the relationship between A$_{40}$ and A$_{42}$ levels in AM (black) and AM;Serf2$^{br-/-}$ (grey) mice at 3 mo of age (detailed statistics in Table S4). (F) Quantification of the A deposits in the region of interest (ROI) of 6E10 immunostained sagittal brain sections from 1- and 3-mo-old AM and AM;Serf2$^{br-/-}$ mice (black line = mean, one-way ANOVA between genotypes at both ages, Bonferroni corrected post-hoc between AM and AM;Serf2$^{br-/-}$ not significant). Right panel: correlation plot depicting the relationship between A$_{40}$ levels and 6E10 plaque density in AM (black) and AM;Serf2$^{br-/-}$ (grey) mice at 3 mo of age. (G) Quantification of the A deposits in the ROI of W0-2 immunostained sagittal brain sections from 1- and 3-mo-old AM and AM;Serf2$^{br-/-}$ mice (black line = mean, one-way ANOVA between genotypes at both ages, Bonferroni corrected post-hoc between AM and AM;Serf2$^{br-/-}$ not significant). Right panel: correlation plot depicting the relationship between A$_{40}$ levels and W0-2 plaque density in AM (black) and AM;Serf2$^{br-/-}$ (grey) mice at 3 mo of age. (H) Quantification of the plaque density in the ROI of Thioflavin-S-stained sagittal brain sections from 1- and 3-mo-old AM and AM;Serf2$^{br-/-}$ mice (black line = mean, One-way ANOVA between genotypes at both ages, Bonferroni corrected post-hoc between AM and AM;Serf2$^{br-/-}$ not significant). Right panel: correlation plot depicting the relationship between A$_{40}$ levels and ThS plaque density in AM (black) and AM;Serf2$^{br-/-}$ (grey) mice at 3 mo of age. In all panels, ROI = cortical and hippocampal area; For all dot plots: WT = black, Serf2$^{br-/-}$ = light grey, AM = dark grey and AM;Serf2$^{br-/-}$ = white; For correlation plots: AM = black and AM;Serf2$^{br-/-}$ = grey, detailed statistics in Table S4; **$P$ < 0.001; *$P$ < 0.01; $P$ < 0.05.
Source data are available for this figure.

expression in our Serf2$^{flox/flox}$ mice (t test WT versus Serf2$^{br-/-}$ brain: 1m $P$ = 0.0022; 3m $P$ = 0.00527) (Figs 3B and C and S2A). The small traces of Serf2 expression detected in the brains of the KO mice is most likely because of the presence of cells from non-neuronal lineage in the samples, for example, cells from the circulatory system. In correspondence with the findings from the full-body KO, we did observe an overall reduction in the brain weight of Serf2$^{br-/-}$ of around 10% compared with WT (two-way ANOVA: genotype $P$ < 0.0001) (Fig 3D). This difference was already present at 1 mo of age and remained at least up to the age of 11 mo. Both WT and Serf2$^{br-/-}$ displayed similar increases in brain weight between 1 and 3 mo of age because of ongoing brain maturation (two-way ANOVA: interaction $P$ = 0.8951). This suggests that the reduction in brain size takes place during an early stage of brain development, but that these changes do not necessarily alter continued development. Additional histological examination of the brains with hematoxylin–eosin staining revealed no difference in the cell density (Fig S2F), nor did we find any evidence of degeneration, apoptosis or necrosis. Apart from the overall reduction in weight, the brains showed no structural abnormalities and the tissue

appeared healthy. We also examined the Sox1-Cre mice (Takashima et al, 2007) without floxed Serf2 ($Cre^{br}$) to distinguish between the effects of Cre expression and $Serf2^{br-/-}$. The $Cre^{br}$ mice also displayed a reduction in brain weight compared with the WT controls (two-way ANOVA: genotype $P = 0.0001$) (Fig 3E), but overall, it was less pronounced than in $Serf2^{br-/-}$ animals. Therefore, it is possible that the expression of Cre alone contributed to the observed decrease in brain size. Overall, brain deletion of SERF2 did not affect the viability or structural integrity of the brain.

### Brain-specific deletion of *Serf2* show no major neurological defects

Next, we performed extensive phenotyping of the $Serf2^{br-/-}$ to investigate basic neurologic functioning, motor function, and behavior (Fig 4). The most prominent difference we observed in our brain-specific deletion model was an overall reduction in body weight compared with WT mice, around 8% for females and 15% for males. In addition, the $Serf2^{br-/-}$ mice appeared slightly more agitated as evidenced by the increased tail elevation and defecation in the SHIRPA (Fig 4, basic neurology panel). The $Serf2^{br-/-}$ mice were also more likely to refrain from a secondary response in the hot plate test within the test period of 30 s, which could indicate altered or retarded thermoreception. However, we cannot exclude that this phenotype was confounded by alterations in other functions. In the tests for motor functions, $Serf2^{br-/-}$ mice show a reduced tendency to passive rotation and reduced latency to falling for both sexes. Although this could indicate a motor deficit, none of the other motor tests consistently demonstrated a motor defect across sexes and measured parameters. Moreover, behavioral differences may also influence rotarod performance and could therefore be the basis of the observed difference. In the behavioral assays, we observed a clear difference in the open field measures for distance travelled and center time, again indicating a hyperresponsiveness to mild novelty stress. In the other behavioral tests, we also observed some mild differences in certain parameters, such as decreased percentage of spontaneous alternations in the Y-maze, reduced social affinity, altered acoustic startle at specific amplitudes, and reduced pre-pulse inhibition, but only at the lowest interstimulus interval. Overall, the latter changes appear less robust and require confirmation in an independent cohort. Although the difference in brain and body size is definitely a factor to be considered during further analysis, our extensive phenotyping of $Serf2^{br-/-}$ mice revealed no major deficits in neurological or motor function and only revealed some mild behavioral alterations, predominantly a slight hyperresponsiveness and increased agitation. Therefore, we decided to proceed with these brain-specific knockout mice to investigate the effect of $Serf2^{br-/-}$ on A brain pathology.

### Brain-specific deletion of SERF2 in APPPS1 mice preserves APP levels or A$\beta$ production

Conditional $Serf2^{br-/-}$ mice were crossed with the APPPS1-21 amyloid (AM) model (Radde et al, 2006), which contains human transgenes for both APP with the Swedish KM670/671NL mutation and PSEN1 with the L66P mutation. From this cross, we obtained four experimental groups: WT, $Serf2^{br-/-}$, AM, and AM;$Serf2^{br-/-}$ (Fig 5A). Upon crossing of the $Serf2^{br-/-}$ with the amyloid model, we observed the expected Mendelian ratio for all the genotypes at P22, indicating that the viability of AM mice was not affected by brain-specific deletion of Serf2 (Chi Square: $P = 0.37$) (Table S3). Based on the known progression of A plaque pathology in the AM mice, we selected two age groups for further analysis: before (1 mo) and after (3 mo) A plaque deposition (Fig 5B). Analysis of the Serf2 mRNA and protein levels in both age groups showed that Serf2 expression was not altered by the A pathology (Two-way ANOVA: $Serf2^{br-/-}$ and AM; $Serf2^{br-/-}$ versus WT 1m $p_{post} < 0.001$; 3m $p_{post} < 0.0001$) (Fig S2B and C). The $Serf2^{br-/-}$ and the AM;$Serf2^{br-/-}$ mice again exhibited the reduction in brain weight previously observed with $Serf2^{br-/-}$ (two-way ANOVA: $Serf2^{br-/-}$ versus WT both ages $p_{post} < 0.01$; AM;$Serf2^{br-/-}$ versus WT 1m $p_{post} < 0.0001$; 3m $p_{post} < 0.001$) (Fig S2D). Also, $Cre^{br}$ mice again showed a similar, albeit slightly less pronounced reduction in brain size (Fig S2E) and hematoxylin–eosin staining revealed no difference in the cell density (Fig S2F) or tissue health because of Serf2 deletion.

Next, we examined whether the brain KO of Serf2 affected any of the key components in the A aggregation process, like altering the levels of APP or the production of its cleavage products, $A_{40}$ and $A_{42}$. We determined the expression of human APP in WT, $Serf2^{br-/-}$, AM, and AM;$Serf2^{br-/-}$ mice at both 1 and 3 mo of age and observed no difference because of brain-specific Serf2 KO (t test: 1m $P = 0.9170$; 3m $P = 0.9963$) (Fig S2G, data from WT and $Serf2^{br-/-}$ not included because of lack of APP construct and absence of signal). Western blot analysis confirmed there was also no difference in APP protein levels between AM and AM;$Serf2^{br-/-}$ (t test: 1m $P = 0.1157$; 3m $P = 0.5908$) (Fig S2H and I). Further analysis of $A_{40}$ (two-way ANOVA: genotype $P = 0.8841$; age $P < 0.0001$; interaction $P = 0.8841$) (Fig 5C) and $A_{42}$ (two-way ANOVA: genotype $P = 0.7006$; age $P < 0.0001$; interaction $P = 0.6522$) (Fig 5D) showed an increase in concentration between 1 and 3 mo, but this was the same in both AM and AM;$Serf2^{br-/-}$. Given the variability in the A concentrations at 3 mo and the fact that the ratio between these two peptides is known to affect the aggregation process, we also investigated the correlation between these two A levels (Fig 5E). This analysis showed that mice with a high $A_{42}$ concentration display a similarly high $A_{40}$ level, maintaining a comparable $A_{40}/A_{42}$ ratio for both AM and AM;$Serf2^{br-/-}$ animals. Similar to previous observations with MOAG-4 in C. elegans, these data suggest that SERF2 does not affect the levels of APP and its cleavage products, $A_{40}$ and $A_{42}$.

### Serf2 KO alters the amount of A$\beta$ deposits in the brain

We next investigated whether SERF2 affects the A aggregation by performing immunohistological analysis of the A plaque pathology. Initially, we performed a general A staining using the 6E10 antibody directed at the N-terminal amino acid residues 1–16. In accordance with the known progression of A plaque pathology in the amyloid model, we only found A deposits in the 3-mo-old AM and AM;$Serf2^{br-/-}$ mice. As expected, most plaques were found in the cortex, with some pathology beginning to spread to the hippocampus as well (Fig S3A). The A deposits displayed a broad range of sizes, but we found no differences in global morphology between the plaque population found in AM

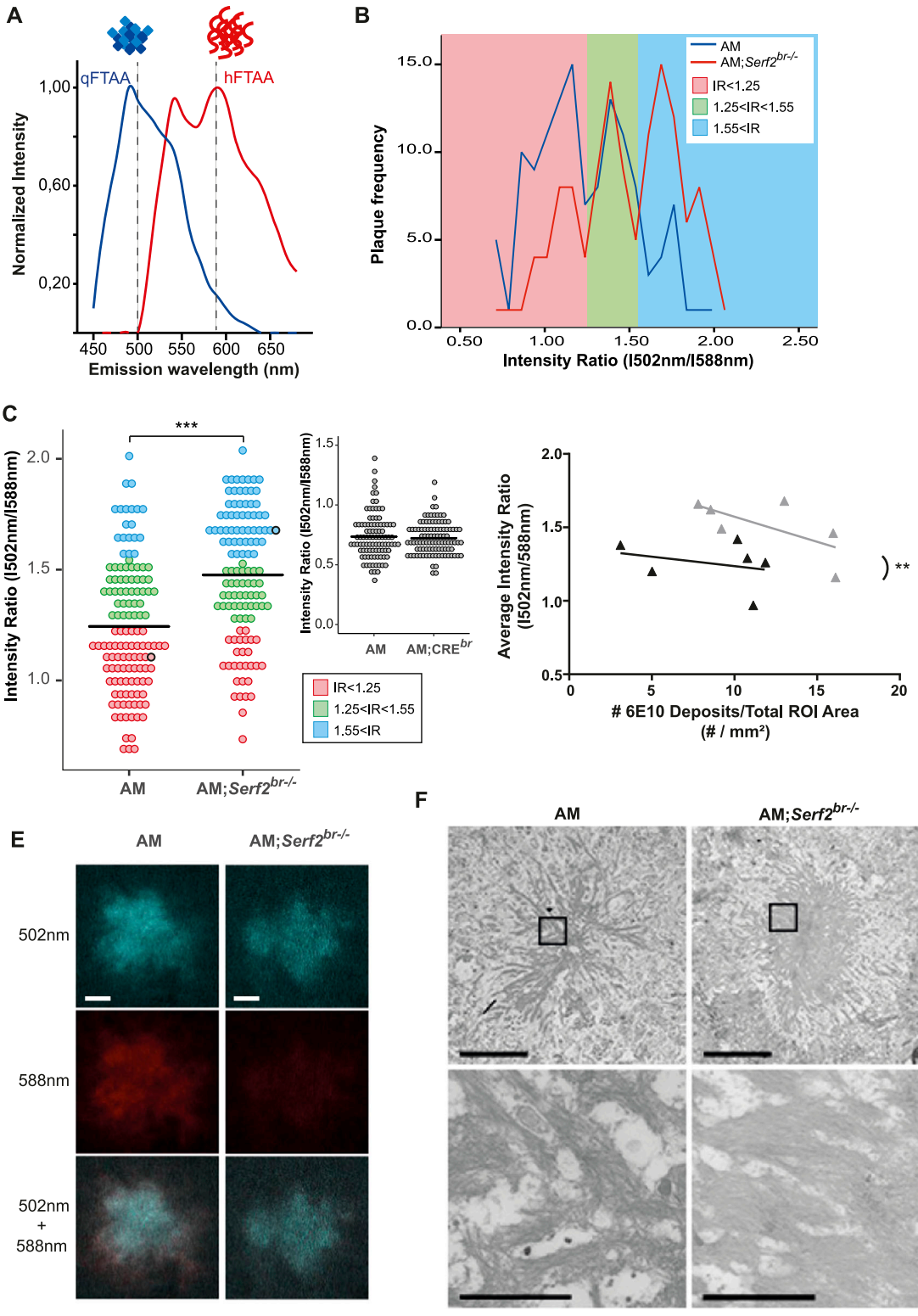


Figure 6. Brain-specific *Serf2* KO alters the structural composition of amyloid plaques.
(A) Graph showing the theoretical LCO dye emission spectra for qFTAA, which binds mature Aβ fibrils (blue), and hFTAA, which binds both mature fibrils and pre-fibrillar Aβ species (red). (B) Frequency distribution of the ratio in fluorescence intensity at 502 nm and 588 nm for all amyloid plaques identified by confocal microscopy in AM (blue) and AM;Serf2$^{br-/-}$ (red) mice at 3 mo of age. Three peak frequency categories were identified: low IR (red), medium IR (green), and high IR (blue) (n = 6 mice/genotype). (B, C, E) Dot plot representing the intensity ratio of all amyloid plaques identified by confocal microscopy for AM and AM;Serf2$^{br-/-}$ mice at 3 mo of age (colors represent the IR categories defined in panel (B), black circles correspond to the plaques depicted in panel (E), black line = mean, t test *** $P < 0.001$) (n = 6 mice/genotype).

and AM;Serf2$^{br-/-}$ (Fig S3B–D). Quantification of the 6E10-positive deposits showed a slight increase in AM;Serf2$^{br-/-}$ compared with AM, but this just failed to reach statistical significance in the Bonferroni corrected post-hoc comparison (two-way ANOVA: all 3m non-AM versus AM groups $p_{bon} < 0.0001$; AM versus AM; Serf2$^{br-/-}$ $p_{bon} = 0.063$) (Fig 5F, left panel). Given the high variability in plaque load between animals within the same experimental group, we examined whether this variability reflected the previously observed variation in A levels. Unsurprisingly, animals with higher levels of A $_{40}$ (Fig 5F, right panel) and A $_{42}$ (Fig S5A) displayed a higher overall plaque load in both groups. More interestingly, our simple linear regression analysis revealed that AM; Serf2$^{br-/-}$ mice tend to have a higher plaque load than AM mice with similar A levels (Table S4). A second A staining with the similar W0-2 antibody, directed at amino acid residues 4–10, displayed a similar slight increase in the amount of plaque deposits in AM;Serf2$^{br-/-}$ at 3 mo (two-way ANOVA: all 3m non-AM versus AM groups $p_{bon} < 0.0001$; AM versus AM;Serf2$^{br-/-}$ $p_{bon} = 0.101$) (Figs 5G, S4, and S5B). In fact, a comparison between 6E10 and W0-2 staining in individual animals confirmed the similarity between both staining patterns at 3 mo (Fig S5C and Table S4). Interestingly, our detection algorithm also picked up a small increase in the counts of W0-2-positive foci in the 1 mo AM; Serf2$^{br-/-}$ group (Two-way ANOVA: 1m WT versus AM;Serf2$^{br-/-}$ $p_{bon} = 0.088$;Serf2$^{br-/-}$ versus AM;Serf2$^{br-/-}$ $p_{bon} = 0.081$; AM versus AM;Serf2$^{br-/-}$ $p_{bon} = 0.127$; all other comparisons $p_{bon} > 0.999$) (Fig 5G, left panel). Closer examination of the microscopic images revealed the identified spots were not extracellular plaques, but were the result of increased levels of W0-2-positive intracellular A staining in AM;Serf2$^{br-/-}$ (Fig S6A). Some low-level intracellular W0-2 and 6E10 staining could also be observed in the other 1-mo-old AM mice, but not to the extent that it was picked up by the detection algorithm (Fig S6A and B). This would suggest that the deletion of Serf2 already alters the intracellular accumulation of A before plaque deposition in a way that affects antibody binding affinity.

To investigate if SERF2 also affected the amount of Thioflavin-positive fibrils, we performed Thioflavin-S (ThS) staining. Here, we again observed a large variety in the amount of ThS-positive plaques between individual animals, but we found no mean difference between AM and AM;Serf2$^{br-/-}$ mice (two-way ANOVA: all 3m non-AM versus AM groups $p_{bon} < 0.001$) (Fig 5H, left panel). However, further analysis of the correlation between A levels and the amount of ThS-positive plaques revealed that AM mice showed a positive correlation similar to the general A staining, whereas AM; Serf2$^{br-/-}$ mice displayed an inverse relationship (Fig 5H, right panel and Table S4). Consequently, a general increase in A deposits does not equate to an increase in ThS-positive amyloid deposition in AM; Serf2$^{br-/-}$ mice, as it does in AM mice (Fig S5D). Combining the unaltered levels of amyloid with changes in the numbers of deposits and their affinity for ThS suggests a change in the amyloid aggregation in Serf2 KO mice.

## Knockout of Serf2 changes the plaque composition and fibril structure

Given the differences in the antibody and ThS binding affinity of the A deposits, we decided to explore the composition within the individual plaques in greater detail. To this end, we made use of two luminescent conjugated oligothiophenes (LCO), small hydrophobic ligands that bind distinct amyloid structures and can easily be distinguished from each other based on their individual spectral properties (Klingstedt et al, 2011). The smallest, qFTAA, has been shown to stain compact, multifilament fibril structures, coinciding with ThT and Congo red staining (Klingstedt et al, 2011; Nyström et al, 2013; Psonka-Antonczyk et al, 2016). The larger hFTAA is capable of staining prefibrillar (non-thioflavinophilic) and single fibril aggregates, also stained with 6E10, but not Congo red, ThT or qFTAA (Klingstedt et al, 2011; Nyström et al, 2013; Psonka-Antonczyk et al, 2016) (Fig 6A). Previous studies have shown that by combining LCO dyes, it is possible to uncover structural differences in plaque composition, which were shown to be associated with different disease phenotypes in patients (Lord et al, 2011; Nyström et al, 2013; Rasmussen et al, 2017). An exploratory frequency analysis of the 502/588 nm intensity ratios plaques in 3-mo-old AM and AM; Serf2$^{br-/-}$ mice revealed a three-peak pattern in which the middle peak was similarly represented in both groups (Fig 6B, green area). The first peak, however, was predominantly found in AM mice (Fig 6B, red area), whereas the third peak was mainly detected in AM; Serf2$^{br-/-}$ (Fig 6B, blue area). This shift in ratio was also reflected by a difference in the average intensity ratio between AM and AM; Serf2$^{br-/-}$ (t test $P < 0.001$) (Fig 6C). This increase in intensity ratio could not be observed in AM;Cre$^{br}$ mice (t test $P = 0.6047$) (Fig 6C, insert), indicating that this effect is caused by the Serf2 KO and unrelated to Cre expression. Given the fact that AM;Cre$^{br}$ animals also show a decrease in brain weight (~8% reduction in AM;Cre$^{br}$ versus ~11% in the AM;Serf2$^{br-/-}$) but do not show similar change in LCO staining, this suggest that the structural changes are also unrelated to the reduction in brain weight. Next, we examined if the change in the intensity ratio correlated with the slight increase in 6E10-positive deposits we observed in AM;Serf2$^{br-/-}$ (Fig 6D). However, the higher average intensity ratio in AM;Serf2$^{br-/-}$ mice was not related to this general plaque load nor the number of W0-2- or ThS-positive deposits (Fig S5E and F). Further microscopic analysis of low-intensity ratio deposits from AM mice showed a plaque with a qFTAA- and hFTAA-positive core and a border that was only stained by hFTAA (Fig 6E, left panels). The high-intensity ratio deposits from AM;Serf2$^{br-/-}$ mice, on the other hand, revealed

(D) Correlation plot depicting the relationship between 6E10 plaque density in the ROI and the LCO average intensity ratio in AM (black) and AM;Serf2$^{br-/-}$ (grey) mice at 3 mo of age (ROI = cortical and hippocampal area, detailed statistics in Table S4) (E) Spectral confocal microscopy images of amyloid plaques in AM and AM;Serf2$^{br-/-}$ mice at 3 mo of age of double stained with qFTAA and hFTAA (top = fluorescence at 502 nm, middle = fluorescence at 588 nm, bottom = merged image of 502 and 588 nm fluorescence, scale bar = 5 m). (F) Scanning transmission electron microscopy pictures of amyloid plaques in the cortex of AM and AM;Serf2$^{br-/-}$ mice at 3 mo of age (top scale bar 5 m, rectangle = zoomed region in bottom picture, bottom scale bar = 1 m). High-resolution EM images are available via http://www.nanotomy.org . Source data are available for this figure.

a qFTAA-positive core, but virtually no hFTAA-staining (Fig 6E, right panels), demonstrating the difference in plaque composition reflected by the shift in LCO intensity ratios. In addition, we visualized the global fibrillar structure of the plaques on a nanometer scale using high-resolution scanning transmission electron microscopy (STEM). Overall, STEM images of plaques from AM;Serf2$^{br-/-}$ tended to show more condensed plaques composed of short, thick, and densely packed bundles of fibers with little space in between (Fig 6F, right panels, and source data of Fig 6). In the AM mice, however, the plaques we observed displayed more loosely packed fibrils (Fig 6F, left panels). Taken together, these findings suggest Serf2 KO in mice leads to a shift in the A aggregation process, resulting in an altered structural composition of the plaques.

## Discussion

Previous studies identified MOAG-4 and its human orthologs SERF1A and SERF2 as modifiers of aggregation of amyloidogenic proteins. In this study, we have demonstrated in cells and mice that SERF2 provides a growth advantage during development. The absence of SERF2 or MOAG-4 in itself does not appear to be lethal in cells, worms or the brain-specific KO mice. Therefore, we postulate that the observed perinatal lethality in the full-body KO mice is a secondary effect of the delay in growth due to insufficient maturation of certain organs at birth, rather than indicating an essential gene function. This appears to be supported by the fact that some pups survived the initial minutes after birth and incomplete penetrance of the lethality in the earliest generations with mixed genetic background. The 129SV genetic background present in these mice is known to have a gestation period that is on average around 1 d longer than C57/Bl6J mice (Murray et al, 2010), which could result in improved lung maturation. These findings are also corroborated by another recent study generating SERF2 KO mice (Cleverley et al, 2021).

The effects of SERF2 on growth and development can be caused by several mechanisms. These mechanisms include the facilitation by SERF2 of cell proliferation directly or it protecting cells from stressors that create an unfavorable environment for cell division, both of which would slow general growth in case of SERF2 depletion. In the latter case, we would expect to see an up-regulation of stress pathways or cell cycle arrest proteins inhibiting the cell cycle in Serf2$^{-/-}$ cells. Interestingly, the RNA-seq analysis of the MEFs from our Serf2$^{-/-}$ mice showed the exact opposite. Cell cycle-driving factors were up-regulated (e.g., cyclins), whereas stress signaling and cell cycle inhibiting factors were down-regulated (e.g., GADD45 and GAS1). Thus, the Serf2$^{-/-}$ cells actually displayed an increased stimulation of cell proliferation mechanisms which would fit with cells from earlier stages of embryonic development. Although the exact endogenous biological function of SERF2 remains unclear, a recent study showed that SERF1a might play a role as an RNA-organizing protein, which localizes to membraneless nuclear organelles, like the nucleolus, under normal physiological conditions. However, under stress conditions, it was shown to migrate to the cytoplasm, where it could drive amyloid toxicity (Meyer et al, 2019 Preprint). Although there was no compensatory up-regulation of SERF1 in response to SERF2 KO and a similar mode of action remains to be demonstrated for SERF2, the region responsible for the RNA-binding properties of SERF1A is highly conserved in MOAG-4 and SERF2 (Meyer et al, 2019 Preprint). Given the importance of nucleolar disassembly and reassembly in cell cycle control (Visintin & Amon, 2000; Leung et al, 2004), a putative RNA-organizing function could explain how SERF2 facilitates cell proliferation, but its precise function in cell proliferation remains to be identified. Loss of SERF2 function in development and cell growth, in addition, would have limited impact in non-proliferating, differentiated cells, like the brain's neurons or the cells of adult C. elegans, and may explain why we saw no adverse effects in the moag-4 deletion worms or our adult Serf2$^{br-/-}$ mice.

In addition, we confirmed the ability of SERF2 to modify the A pathology in vivo in a mouse model without it changing the overall A levels. This finding is in accordance with the previously observed effects of MOAG-4 on the aggregation of polyglutamine, A , and Syn in C. elegans (van Ham et al, 2010). At 1 mo of age, before plaque deposition, we already observe a change in intracellular A accumulation, which resembles the recently reported intracellular, perinuclear accumulation believed to be the precursor for the dense plaque core (Lee et al, 2022). We further showed that mice lacking SERF2 were more prone to form A deposits and that the composition of these deposits was structurally different. In AM mice, higher levels of A result in an increase in the numbers of A deposits and an increase in the number of ThS-positive deposits. AM;Serf2$^{br-/-}$ mice, on the other hand, also show an increase in A deposits, but this did not lead to higher numbers of ThS-positive plaques, indicating an altered dynamic and outcome of amyloid formation. These findings were further corroborated by the LCO spectra, which revealed that the plaques in AM;Serf2$^{br-/-}$ mice have a different conformation of pre- fibrillar and fibrillar A compared with AM mice. Finally, STEM imaging also confirmed a globally altered structure of the amyloid fibrils in the plaques.

Based on previous studies, the LCO spectra observed in brains of Serf2-deletion mice, however, would resemble the spectra of increased mature fibrils (Nyström et al, 2013; Psonka-Antonczyk et al, 2016). If so, this would seemingly contradict findings in previous studies, such as the in vitro aggregation results in Pras et al (2021). However, with a finite amount of aggregating protein, SERF2 mainly acts on nucleation. It is therefore possible that removal of Serf2 could shift the balance in the aggregation kinetics towards elongation and maturation instead of the formation of new nuclei, resulting in more mature fibrils. Further in-depth temporal and structural analyses, including those assessing associations between SERF2 and amyloid in brain, will be required to determine mechanism by which depletion of Serf2 altered the amyloid structures.

Amyloid fibrils are formed through a nucleated self-assembly process characterized by a structural conformation to a -strand secondary structure and the formation of a critical nucleus during the initial oligomerization. The nuclei act as seeds from which the fibrils grow and have been shown to propagate a specific fibril structure (Petkova et al, 2005; Qiang et al, 2017). In vitro kinetic assays SERF and MOAG-4 accelerate aggregation by acting on the nucleation phase (Falsone et al, 2012; Yoshimura et al, 2017; Meinen